ChemPubSoc Europe

DOI: 10.1002/ejic.201900231

EurJIC European Journal of Inorganic Chemistry

Full Paper

Spin Crossover Thin Films

SPECIAL ISSUE

Nanocrystalline Polymer Impregnated [Fe(pz)Pt(CN)$_4$] Thin Films Prepared by Matrix-Assisted Pulsed Laser Evaporation

Mirosław Sawczak,*[a] Rafał Jendrzejewski,[a] Dominik Maskowicz,[a] Yann Garcia,*[b] Astha C. Ghosh,[b] Maria Gazda,[c] Jakub Czechowski,[c] and Gerard Śliwiński[a]

Dedicated to the memory of Dr. Krzysztof Drabent (Wroclaw)

Abstract: In this work, the fabrication of [Fe(pz)Pt(CN)$_4$] (pz = pyrazine) thin films by means of matrix-assisted pulsed laser evaporation (MAPLE) was investigated. As starting material, a cryogenically cooled suspension of nanocrystalline [Fe(pz)Pt(CN)$_4$] (0.35wt.-%) in a mixture of *1,1*-dichloroethane and polyethylene glycol (PEG) was used. Films of a thickness up to 150–200 nm were deposited on Si substrates by laser ablation at λ = 1064 nm of the cryogenically cooled material. PEG impregnated films exhibit a cooperative first-order hysteretic spin crossover behavior around 155 K as detected by Raman spectroscopy. Most interestingly, deposition of a crystalline material was achieved through MAPLE deposition.

Introduction

Metal-organic frameworks (MOFs) are widely investigated materials due to their unlimited chemical design,[1] and their variety of potential applications such as sensors,[2] drug carriers,[3] semiconductors,[4] mercury storage,[5] and many more. Among MOFs and coordination polymers, those that display spin crossover (SCO) behavior can be distinguished. In particular, Fe^{II} complexes including bis-1,2,4-triazole[6,7] or bis-tetrazole ligands, which have been the first to be investigated,[8] within this substance class. 3D Hoffman-like Fe^{II} cyanide networks, of general formula {FeL$_x$[M(CN)$_4$]}•Solv with M = Ni, Pt, Pd and {FeL$_x$[M(CN)$_2$]$_2$}•Solv with M = Ag, Au, have been however the most studied among SCO MOFs. This is due to their remarkable magnetic and thermochromic behavior, often occurring around the room temperature region.[9] Because the SCO is accompanied by easily detectable macroscopic changes,[10] such materials bear strong potential for information storage, low energy displays and sensing applications.[11–13]

Their implementation into devices is however challenging due to the fragility of their SCO profiles in the solid state, which are highly dependent on the material processing environment. Therefore, great efforts have been made towards their controlled implementation as thin films and nanoparticles. The most popular methods to obtain SCO thin films include Langmuir–Blodgett deposition,[14] dip coating,[15] spin coating,[16] drop casting,[17] constructive methods,[18] electrodeposition,[19] dispersion into polymers,[20] intercalation in layered materials[21] and capillary deposition.[22] Vacuum sublimation methods, such as e.g. Chemical Vapor Deposition (CVD) and Physical Vapor Deposition (PVD),[23] have also been applied. Among PVD methods, pulsed Laser Deposition (PLD) has greatly developed,[24] although it has not yet been considered in SCO research. Among such deposition methods, the matrix-assisted pulsed laser evaporation (MAPLE) can be distinguished due to its superior characteristics for the study of fragile materials.[25] Indeed, under properly selected conditions the laser beam is absorbed exclusively by the matrix (solidified solvent). As a consequence, any fragile guest material becomes protected against excessive irradiation, overheating and thermal damage, thus preserving its chemical composition and molecular structure.[25] MAPLE allows deposition of polymeric, organic or biological structures and other materials vulnerable to high temperature.[26] Due to such interesting properties, we thought to apply the MAPLE deposition technique for processing a molecular complex displaying SCO, for the first time. Our interest was directed to the 3D Hofmann like cyanide network, [Fe(pz)Pt(CN)$_4$] (pz = pyrazine). This compound has indeed received a paramount attention not only because of its outstanding SCO properties associated with a large hysteresis width centered at room temperature for powder and film samples,[18,27] bidirectional light-switching,[27] and its sensing potential for various gases,[28] but also for its ability to be prepared as nanoparticles,[29] as well as nanometric patterns.[30]

The crystallinity of the starting material,[29a] is considered as an asset for thin film deposition, whereas the film quality and

[a] *Institute of Fluid-Flow Machinery, Photophysics Dept., Polish Academy of Sciences, 14 Fiszera St., 80–231 Gdańsk, Poland E-mail: mireks@imp.gda.pl, gerards@imp.gda.pl http://www.imp.gda.pl*

[b] *Institute of Condensed Matter and Nanosciences, Université catholique de Louvain, Place L. Pasteur 1,1348 Louvain-la-Neuve, Belgium E-mail: yann.garcia@uclouvain.be*

[c] *Faculty of Applied Physics and Mathematics, Gdańsk University of Technology, 11/12 Narutowicza St, 80–233 Gdansk, Poland*

Supporting information and ORCID(s) from the author(s) for this article are available on the WWW under https://doi.org/10.1002/ejic.201900231.

properties both depend strongly on the deposition conditions.[31] A common issue concerns however the poor adhesion of nanometer size crystals to the substrate surface. This drawback can impact negatively the film growth and its homogeneity, and thus result in decreased film functionality.[31] In order to overcome this issue, layers covering of the substrate may be needed or addition of a surfactant to the MAPLE target solution. The use of pulsed laser for processing such fragile Hofmann-type 3D framework is also considered as challenging since it would request a careful selection of interaction parameters in order to avoid decomposition of the SCO material,[32] and could be very time consuming.

Considering all these parameters, film fabrication of $[Fe(pz)Pt(CN)_4]$ was undertaken under various conditions. Polymer addition (e.g. polyethylene glycol, PEG) was used to enhance adhesion of the nanocrystalline material to the Si substrate and the effect of the PEG presence on the growth and properties of the film were investigated. The SCO properties of the new thin film made of $[Fe(pz)Pt(CN)_4]$ were investigated and compared to the one of the reference nanomaterial, using temperature dependent Raman spectroscopy.

Results and Discussion

Film Preparation

The base target for laser ablation was prepared by suspending a nanocrystalline powder of $[Fe(pz)Pt(CN)_4]$ in *1,1*-dichloroethane. This solvent was selected due to maximal absorption revealed for the applied laser irradiation at $\lambda = 1064$ nm. Moreover, the polymer enriched target was prepared by admixture of PEG to the nanoparticle suspension and thoroughly mixed. PEG was chosen due to its relatively high viscosity and adequate solubility in common solvents. It was applied both as surfactant for SCO nanoparticles[33] and as an adhesion layer covering the Si substrate. Both suspensions were solidified at cryogenic temperature (90–100 K) and served as targets in the MAPLE process as shown in Scheme 1.

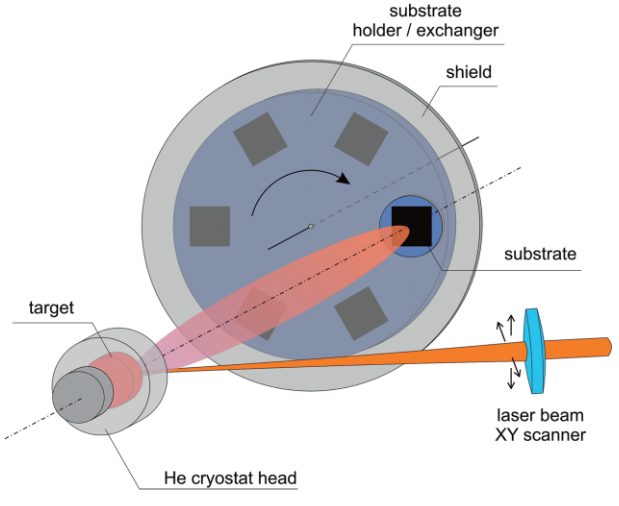

Scheme 1. MAPLE experimental setup applied for thin film deposition of the nanocrystalline $[Fe(pz)Pt(CN)_4]$.

The deposition was carried out under vacuum conditions (10^{-6} mbar). Thin films were fabricated on Si platelets (1×1 cm^2) mounted at a distance of 35 mm from the target surface and preheated at temperatures in the range of 293–323 K in order to prevent condensation of the solvent originating from droplets of the molten target. During the ablation process the target surface has been scanned by the focused laser beam in order to avoid crater formation.

Thin Film Structure and Characterization

The effect of polymer addition on the structure of MAPLE deposited thin film has been investigated for four samples **S1**–**S4** shown and described in Scheme 2. **S1** was deposited by laser evaporation of the solidified suspension of nanocrystalline $[Fe(pz)Pt(CN)_4]$ in *1,1*-dichloroethane directly on the Si substrate. Relatively small, irregularly distributed islands (nanoparticle agglomerates) accompanied by circular traces of evaporated solvent drops are seen in the optical microscope image of **S1**, thus revealing a weak surface coverage (Figure 1). The application of a thin PEG layer prior to deposition of the molecular complex, as performed for samples **S2** and **S4**, resulted in a visible difference in comparison to **S1**. Indeed, even the relatively large, ablated target fragments reaching the Si surface become immobilized which results in improved film density (Figure 1). Even sample **S3** revealed a superior substrate coverage characterized by nearly homogeneous distribution of the nanoparticle material.

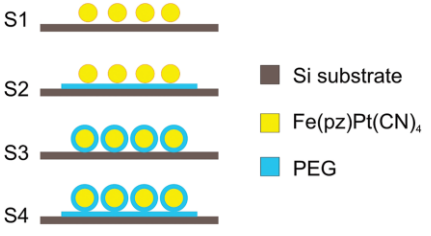

Scheme 2. Layout of the MAPLE deposited samples: **S1** – $[Fe(pz)Pt(CN)_4]$ deposited on silicone substrate, **S2** and **S4** – deposition on Si substrate already coated with a PEG layer, **S3** and **S4** – films of PEG impregnated by $[Fe(pz)Pt(CN)_4]$ suspended in *1,1*-dichloroethane.

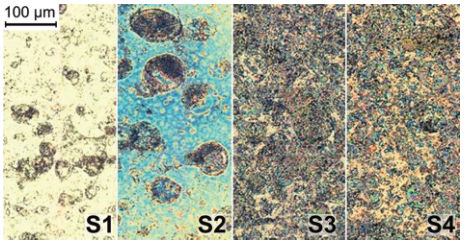

Figure 1. Optical microscope images of the MAPLE deposited samples **S1**–**S4**.

This observation is confirmed by X-ray fluorescence (XRF) analysis of the deposited thin films which show a relative Pt content three times higher in **S3** and **S4** compared to **S1** and **S2** (Figure 2). The effect of PEG precoating applied on the substrate surface, thought on **S2**, is practically negligible. This re-

sult is in agreement with profilometer measurements of the film thickness and surface roughness shown in Figure 3 which additionally show that the improvement of the film density due to PEG presence is accompanied by an increased film thickness from ca. 100 nm (**S1**) to 150–200 nm (**S3** and **S4**).

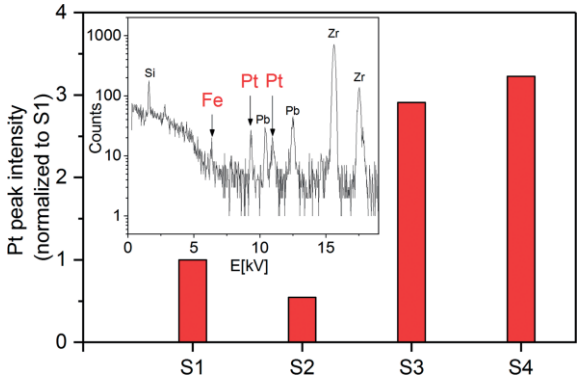

Figure 2. Relative XRF peak intensities of the Pt content related to the corresponding to nanomaterial density in the thin films **S1**–**S4**.

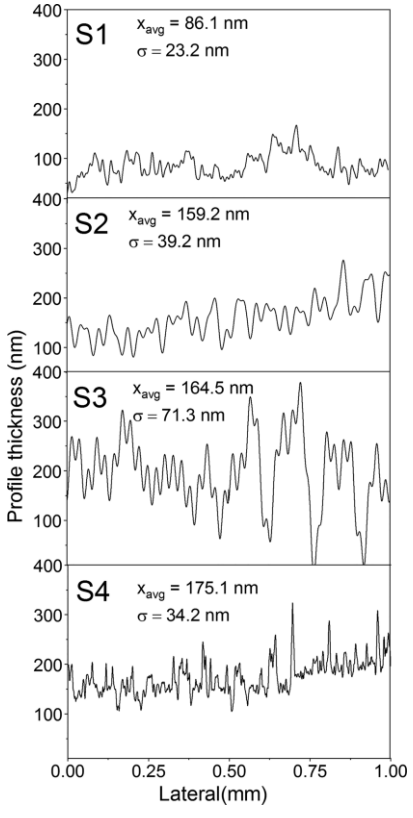

Figure 3. Surface profiles for **S1**–**S4** showing film thickness and surface roughness.

The film surface structures of **S1** and **S3** (as the examples of films obtained for nanopowder without and with PEG layer, respectively) were investigated by SEM (Figure 4), in addition to the reference material which show relatively more deposited material. The crystalline material is partially immersed in the case of polymer film **S3** because the polymer used as an additive in the target preparation is transported to substrate and

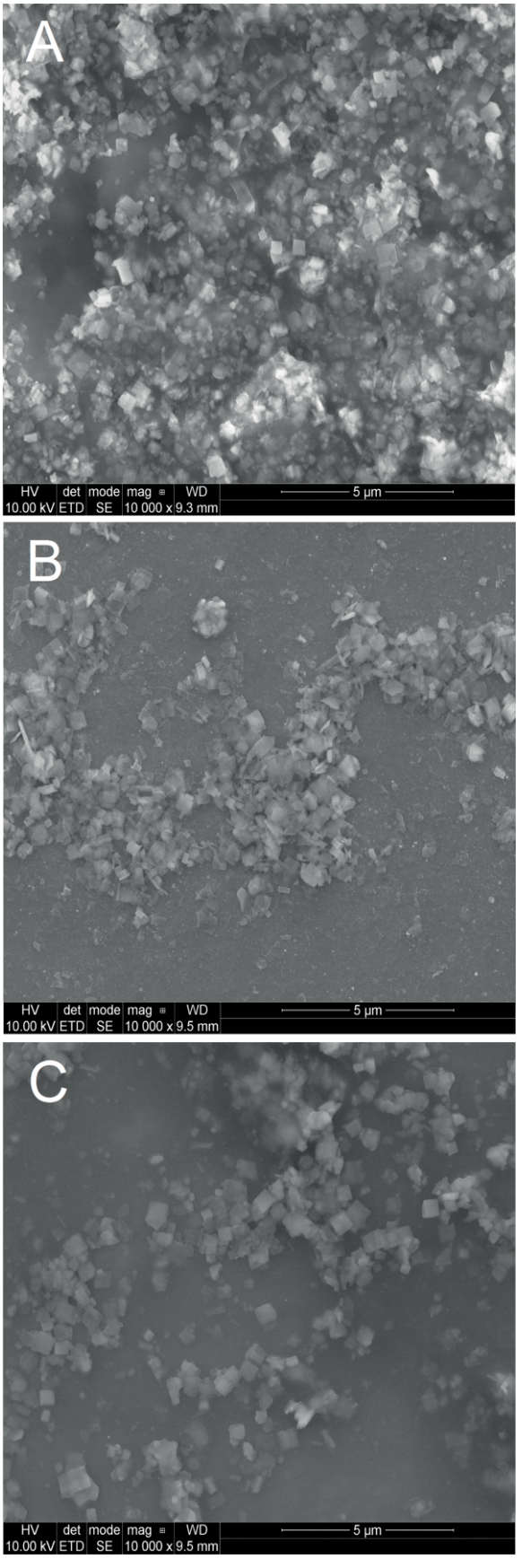

Figure 4. SEM images of $[Fe(pz)Pt(CN)_4]$ reference material (A), and films **S1** (B) and **S3** (C).

deposited together with [Fe(pz)Pt(CN)$_4$] nanoparticles. The number of deposited nanocrystals is lower for **S1**, where the deposition process was carried out without polymer added to the target material, compared to **S3** for polymer covered nanocrystals, where particles stick to each other more efficiently, which results in increased film density.

Based on optical microscopy and SEM inspection as well as profilometry and XRF measurements, it can be concluded that the results obtained for samples **S3** and **S4** are much better than in the case of **S1** and **S2**. On the other hand the surface structures of samples **S4** and **S3** are comparable and therefore more extensive results obtained for **S3** sample are discussed below.

The crystallinity of the MAPLE deposited films has been examined by comparison of X-ray diffraction data obtained for the film **S3** and the reference sample of [Fe(pz)Pt(CN)$_4$] (Figure 5). The XRD pattern of the film reveals indeed all characteristic reflexions and is in agreement with that measured for the nanocrystalline reference material. Exception is found for the Si peak due to different substrates applied and a small shift observed (of instrumental origin) for the entire spectrum. This implies that the applied laser radiation has no destructive effect on the crystalline structure of the deposited nanoparticles. Similar conclusion may be drawn from analysis of the Raman spectra obtained for samples **S1–4** and the reference nanocrystals - see Figure S1 in Supporting Information.

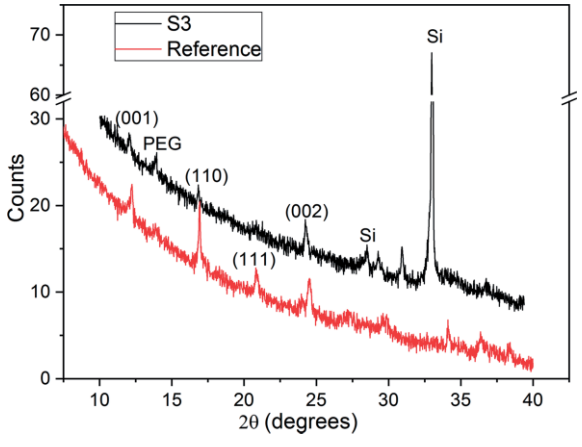

Figure 5. XRD diffractograms of the reference sample of [Fe(pz)Pt(CN)$_4$] and of the thin film **S3**.

Spin Crossover Behavior of Polymer Impregnated MAPLE Film

Temperature dependent micro-Raman spectra of MAPLE thin film **S3** as well as for the reference nanocrystalline sample of [Fe(pz)Pt(CN)$_4$] were studied over the temperature range 300–80 K in the 590–2500 cm^{-1} frequency region. Spectra recorded at 280 K and 100 K, which correspond to the temperatures where the nanocrystalline material is in the high-spin (HS) and in the low-spin (LS) state, respectively, are shown in Figure 6.[29a] Both spectra reveal a well resolved doublet around 2200 cm^{-1}, corresponding to the CN stretch,[33] whereas another signal is found at 1030 cm^{-1}, corresponding to the breathing mode of the bridging pyrazine.[34] The presence of well defined peaks in nanocrystalline thin film confirms that the crystallinity of the deposited sample is not lowered, as noticed by X-ray diffraction (Figure 5). This result is of the utmost importance compared to classic sublimation methods of SCO complexes,[23] which usually lead to a decrease or even a complete disappearance of the crystallinity of deposited materials.[35] Remarkable differences in band intensities assigned to pyrazine modes at ca. 1230 and ca. 1600 cm^{-1} were noticed, on going from the HS to the LS state (Figure 6).[18] A temperature dependent band shift was observed in the range 600–700 cm^{-1}, suggesting the occurrence of a SCO behavior, as observed by Bonhommeau et al.[27] The intensity ratio of the noticeable Raman modes at 1030 cm^{-1} and 1233 cm^{-1} was selected to plot the SCO curve in both cooling and warming modes (Figure 7).[18] A collection of Raman spectra recorded for both **S3** and reference nanocrystalline samples at intermediate temperatures between the low and high spin state are presented in Figure S2, Supporting Information. The thin film **S3** reveals a hysteretic loop, characteristic of a thermally induced SCO behavior with $T_{1/2}{}^{\downarrow}$ = 143 K and $T_{1/2}{}^{\uparrow}$ = 171 K. Surprisingly, a downshift of the hysteresis loop of ca. 150 K is observed when compared to the reference material with transition temperatures $T_{1/2}{}^{\downarrow}$ = 274 K and $T_{1/2}{}^{\uparrow}$ = 284 K (Figure 7). This temperature shift corresponds to a negative pressure as earlier observed for instance for [Fe(hyptrz)$_3$](4-chloro-3-nitrophenylsulfonate)$_2$•2H$_2$O (hyptrz = 4-(3′-hydroxypropyl)-1,2,4-triazole), when embedding this 1D SCO material into silicon oil.[36] This contrasts with the thin films obtained by multilayer sequential assembly of the title material, whose SCO curve was slightly shifted upwards room temperature compared to the powdered material.[18] It is also interesting to notice that the SCO proceeds in a smoother fashion, compared to the nanocrystalline reference material, which results in the observed asymmetric hysteresis loop combined with its widening from 10 K to 28 K.

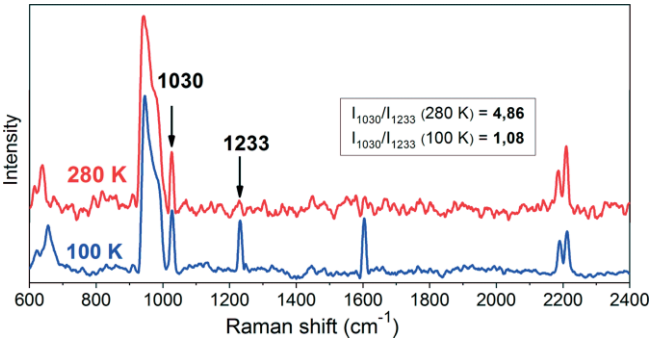

Figure 6. Stack plotted Raman spectra of the thin film **S3** at 280 K and 100 K with the corresponding difference in the intensity ratios for selected bands.

The modification on the SCO curve cannot be associated with changes of the crystallinity or a structural phase transition,[37] since a good match was obtained between thin film **S3** and reference nanomaterial by X-ray diffraction (Figure 5). Also, no line broadening was observed in the Raman spectra.[35] Presumably, the observed change in SCO behavior results both from the observed particle size reduction in the thin film,[29a] and the interaction at the substrate-film interface as recently

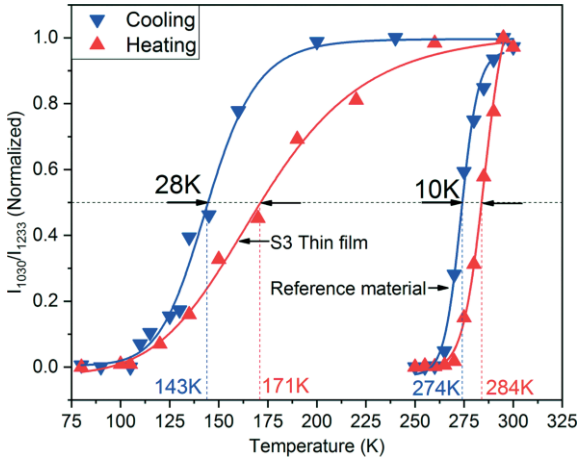

Figure 7. Temperature dependence of the relative Raman band intensities upon heating (red) and cooling (blue) for thin film **S3** and reference nanocrystalline sample of $[Fe(pz)Pt(CN)_4]$.

reported by Delgado et al.[38] An excessive laser irradiation energy would result in a complete removal of structural water and/or pyrazine molecules, which can even lead to the framework collapse.[39] Both effects can however be excluded, since the first one would not lead to a positive pressure effect, as observed by Bonhommeau et al.,[27] whereas the second one would lead to a network alteration, which has not been confirmed by X-ray diffraction (Figure 5). An hydration occurring after the thin film deposition would seem reasonable since such phenomenon is known to produce a shift to lower temperatures for the title compound.[27] The similar influence of polymer matrix on spin crossover temperatures was also observed and discussed by Tanasa et al. for $Fe(phen)_2(NCS)_2$ microparticles embedded in glass-forming or semicrystalline matrices.[40] These authors ascribe the modification of the SCO material properties to interactions with the matrix which in turn depend on mechanical properties of the latter.

Conclusions

The laser based MAPLE deposition process has been successfully carried out to prepare thin films of a nanocrystalline spin crossover material, for the first time. To support the adhesion of nanocrystalline particles on the substrate surface and the film growth, polyethylene glycol was applied as surfactant. Films of a thickness from 100 nm (without polymer) up to 200 nm were deposited on pure and polymer coated Si substrates by nanosecond laser ablation. The polymer addition to the MAPLE target acted as surfactant and influenced positively both the film growth and homogeneity, as concluded from optical and SEM inspection. Polymer impregnated films exhibit an hysteretic first-order phase transition around 150 K evidenced by variable temperature Raman measurements. More importantly, crystallinity is preserved after deposition in contrast to other deposition methods. Such study opens the way to further MAPLE thin film fabrication of spin crossover materials and other functional metal-organic frameworks.

Experimental Section

Materials: $Fe(BF_4)_2{\cdot}6H_2O$, $K_2[Pt(CN)_4]$ and pyrazine were obtained from Sigma-Aldrich and used as received. Sodium bis(2-ethylhexyl) sulfosuccinate (NaAOT) and octane were obtained from TCI and used without further purification. Polyethylene glycol (PEG) and *1,1*-dichloroethane were used as received from Sigma-Aldrich and used as received.

Synthesis of nanocrystalline $[Fe(pz)Pt(CN)_4]$: $[Fe(pz)Pt(CN)_4]$ nanocrystals were synthesised in water-in-oil microemulsions using the procedure established by Real et al.[29a] It involved $Fe(BF_4)_2{\cdot}6H_2O$, $K_2[Pt(CN)_4]$, pyrazine for the synthesis of the complex and NaAOT to stabilize microemulsions. Deionized water was deoxygenated by sonication and Ar bubbling during 1 h.

Target and substrate preparation: Silicon substrates were sonicated in acetone, rinsed with 2-propanol and dried with pressurized air before use. $[Fe(pz)Pt(CN)_4]$ nanocrystalline powder (1.2 mg) was dispersed in *1,1*-dichloroethane (0.6 mL) to form a homogeneous suspension for **S1** and **S2**. For samples **S3** and **S4**, a mixture of the complex dissolved in *1,1*-dichloroethane and PEG with PEG:$[Fe(pz)Pt(CN)_4]$ ratio of 1:1 was used to achieve a nanomaterial concentration 0.35 % in suspension sonicated for 15 min. PEG films on substrates for samples **S2** and **S4** were drop-casted with 100 μL of 0.35 % PEG in *1,1*-dichloroethane solution.

MAPLE deposition: Prior to the film fabrication, Si substrates were mounted on a rotating holder, inside vacuum chamber at backing pressure of 10^{-6} bar. Next, the liquid suspension was poured into the cryo-vessel and left for solidification at 80 K using a He-cryostat (Leybold). Distance between substrate and target was set to 35 mm. A pulsed laser Briliant B (Quantel, λ = 1064 nm, 6 ns pulse duration) was focused on the target by a quartz lens controlled by stepper motors that allowed uniform rastering of the target surface in order to avoid crater formation. The laser beam intensity (pulse frequency 10 Hz) at the target surface was set to 2 J/cm^2 and the deposition time of a single thin film sample was limited to 60 min for all samples. The deposited film samples were demounted from holder after filling the chamber with nitrogen up to atmospheric pressure.

Instruments and methods: XRD data were collected with the X' Pert Phillips diffractometer with Cu K-α radiation (λ = 1.541 Å). **Raman** spectra were acquired with a micro-Raman spectrometer (inVia™, Reinshaw) equipped with $N_{2(l)}$ cryostat module Optistat (Oxford Instruments). Samples were excited at λ = 785 nm (ModuLaser™) using a laser power less than 0.1 mW. To avoid water condensation during measurements, $[Fe(pz)Pt(CN)_4]$ films were covered with a glass (0.15 mm thick) and sealed with a hot press lamination using thermoplastic 60 μm thick gasket (Surlyn, DuPont). Spectra were recorded over the frequency range of 550–2400 cm^{-1} for temperatures selected between 320–100 K at 10 K intervals. **SEM** inspection was performed with a FEI (Quanta) FEG 250 Scanning Electron Microscope. **XRF** data were collected by means of a custom build system equipped with a X-ray tube operating at 55 kV (1 mA) and a SDD detector (155 eV resolution for Mn K_α). **Profilometry** measurements were performed with a mechanical profilometer Dektak XT, Bruker.

Acknowledgments

Authors acknowledge financial support from the FNRS-PAN and WBI-MNiSW joint research projects, FNRS PDR T.0102.15, FNRS CDR 33694457 and collaboration in the frame of the COST Action CA15129 MOLSPIN. We thank Dr. M. M. Dîrtu for her involvement in the early stages of this work.

Keywords: Spin crossover · Iron · Nanoparticles · Thin films · Laser deposition · Nanostructuration · Spintronic devices

[1] S. Kitagawa, *Chem. Soc. Rev.* **2014**, *43*, 5415–5418.
[2] L. E. Kreno, K. Leong, O. K. Farha, M. Allendorf, R. P. Van Duyne, J. T. Hupp, *Chem. Rev.* **2012**, *112*, 1105–1125.
[3] R. C. Huxford, J. Della Rocca, W. Lin, *Curr. Opin. Chem. Biol.* **2010**, *14*, 262–268.
[4] C. G. Silva, A. Corma, H. García, *J. Mater. Chem.* **2010**, *20*, 3141–3156.
[5] N. N. Adarsh, M. M. Dîrtu, A. D. Naik, A. F. Léonard, N. Campagnol, K. Robeyns, J. Snauwaert, J. Fransaer, B. L. Su, Y. Garcia, *Chem. Eur. J.* **2015**, *21*, 4300–4307.
[6] Y. Garcia, V. Niel, M. Carmen-Munoz, J. A. Real, *Top. Curr. Chem.* **2004**, *233*, 229–257.
[7] a) Y. Garcia, O. Kahn, L. Rabardel, B. Chansou, L. Salmon, J. P. Tuchagues, *Inorg. Chem.* **1999**, *38*, 4663–4670; b) Y. Garcia, N. N. Adarsh, A. D. Naik, *Chimia* **2013**, *67*, 411.
[8] a) P. J. van Koningsbruggen, Y. Garcia, H. Kooijman, A. L. Spek, J. G. Haasnoot, O. Kahn, J. Linares, E. Codjovi, F. Varret, *J. Chem. Soc., Dalton Trans.* **2001**, *4*, 466–471; b) C. M. Grunert, J. Schweifer, P. Weinberger, W. Linert, K. Mereiter, G. Hilscher, M. Müller, G. Wiesinger, P. J. van Koningsbruggen, *Inorg. Chem.* **2004**, *43*, 155–165; c) G. Aromí, L. A. Barrios, O. Roubeau, P. Gamez, *Coord. Chem. Rev.* **2011**, *255*, 485–546.
[9] a) M. C. Muñoz, J. A. Real, *Coord. Chem. Rev.* **2011**, *255*, 2068–2093; b) F. J. Valverde-Muñoz, M. C. Muñoz, S. Ferrer, C. Bartual-Murgui, J. A. Real, *Inorg. Chem.* **2018**, *57*, 12195–12205.
[10] P. Gütlich, A. B. Gaspar, Y. Garcia, *Beilstein J. Org. Chem.* **2013**, *9*, 342–391.
[11] J. Linares, E. Codjovi, Y. Garcia, *Sensors* **2012**, *12*, 4479–449.
[12] A. Holovchenko, J. Dugay, M. Giménez-Marqués, R. Torres-Cavanillas, E. Coronado, H. S. van der Zant, *Adv. Mater.* **2016**, *28*, 7228–7233.
[13] M. M. Dîrtu, A. D. Naik, A. Rotaru, L. Spinu, D. Poelman, Y. Garcia, *Inorg. Chem.* **2016**, *55*, 4278–4295.
[14] H. Soyer, C. Mingotaud, M.-L. Boillot, P. Delhaes, *Langmuir* **1998**, *14*, 5890–5895.
[15] K. Kuroiwa, T. Shibata, S. Sasaki, M. Ohba, A. Takahara, T. Kunitake, N. Kimizuka, *J. Polym. Sci., Part A J. Polym. Sci., Part A Polym. Chem.* **2006**, *44*, 5192–5202.
[16] a) M. Matsuda, H. Tajima, *Chem. Lett.* **2007**, *36*, 700–701; b) A. D. Naik, M. M. Dîrtu, Y. Garcia, *J. Phys. Conf., Ser.* **2010**, *217*, 012032.
[17] Y. Galyametdinov, V. Ksenofontov, A. Prosvirin, I. Ovchinnikov, G. Ivanova, P. Gütlich, W. Haase, *Angew. Chem. Int. Ed.* **2001**, *40*, 4269–4271; *Angew. Chem.* **2001**, *113*, 4399.
[18] S. Cobo, G. Molnár, J. A. Real, A. Bousseksou, *Angew. Chem. Int. Ed.* **2006**, *45*, 5786–5789; *Angew. Chem.* **2006**, *118*, 5918.
[19] B. Djukic, M. T. Lemaire, *Inorg. Chem.* **2009**, *48*, 10489–10491.
[20] A. Tissot, J.-F. Bardeau, E. Rivière, F. Brisseta, M.-L. Boillot, *Dalton Trans.* **2010**, *39*, 7806–7812.
[21] a) E. Coronado, M. Giménez-Marqués, C. Martí-Gastaldo, G. Mínguez Espallargas, E. Navarro-Moratalla, J. C. Waerenborgh, *Inorg. Chem.* **2013**, *52*, 8451–8460; b) T. Zhao, L. Cuignet, M. M. Dîrtu, M. Wolff, V. Spasojevic, I. Boldog, A. Rotaru, Y. Garcia, C. Janiak, *J. Mater. Chem. C* **2015**, *3*, 7802–7812.
[22] A. D. Naik, L. Stappers, J. Snauwaert, J. Fransaer, Y. Garcia, *Small* **2010**, *6*, 2842–2846.
[23] a) S. Shi, G. Schmerber, J. Arabski, J.-B. Beaufrand, D. J. Kim, S. Boukari, M. Bowen, N. T. Kemp, N. Viart, G. Rogez, E. Beaurepaire, H. Aubriet, J. Petersen, C. Becker, D. Ruch, *Appl. Phys. Lett.* **2009**, *95*, 043303; b) H. Naggert, A. Bannwarth, S. Chemnitz, T. von Hofe, E. Quandt, F. Tuczek, *Dalton Trans.* **2011**, *40*, 6364–6366; c) T. Palamarciuc, J. C. Oberg, F. El Hallak, C. F. Hirjibehedin, M. Serri, S. Heutz, J.-F. Létard, P. Rosa, *J. Mater. Chem.* **2012**, *22*, 9690–9695; d) M. Bernien, D. Wiedemann, C. F. Hermanns, A. Krüger, D. Rolf, W. Kroener, P. Müller, A. Grohmann, W. Kuch, *J. Phys. Chem. Lett.* **2012**, *3*, 3431–3434; e) T. G. Gopakumar, M. Bernien, H. Nagger, F. Matino, C. F. Hermanns, A. Bannwarth, S. Mühlenberend, A. Krüger, D. Krüger, F. Nickel, W. Walter, R. Berndt, W. Kuch, F. Tuczek, *Chem. Eur. J.* **2013**, *19*, 15702–15709; f) M. Bernien, H. Naggert, L. M. Arruda, L. Kipgen, F. Nickel, J. Miguel, C. F. Hermanns, A. Krüger, D. Krüger, E. Schierle, E. Weschke, F. Tuczek, W. Kuch, *ACS Nano* **2015**, *9*, 8960; g) H. Naggert, J. Rudnik, L. Kipgen, M. Bernien, F. Nickel, L. M. Arruda, W. Kuch, C. Näther, F. Tuczek, *J. Mater. Chem. C* **2015**, *3*, 7870; h) K. Bairagi, O. Iasco, A. Bellec, A. Kartsev, D. Li, J. Lagoute, C. Chacon, Y. Girard, S. Rousset, F. Miserque, Y. J. Dappe, A. Smogunov, C. Barreteau, M.-L. Boillot, T. Mallah, V. Repain, *Nat. Commun.* **2016**, *7*, 12212; i) S. Ossinger, H. Naggert, L. Kipgen, T. Jasper-Toennies, R. Torben, R. Abhishek, N. Julian, F. Nickel, L. M. Arruda, M. Bernien, W. Kuch, R. Berndt, F. Tuczek, *J. Phys. Chem. C* **2017**, *121*, 1210–1219; j) X. Zhang, P. S. Costa, J. Hooper, D. P. Miller, A. T. N'Diaye, S. Beniwal, X. Jiang, Y. Yin, P. Rosa, L. Routaboul, M. Gonidec, L. Poggini, P. Braunstein, B. Doudin, X. Xu, A. Enders, E. Zurek, P. A. Dowben, *Adv. Mater.* **2017**, *29*, 1702257; k) V. Shalabaeva, S. Rat, M. D. Manrique-Juarez, A.-C. Bas, L. Vendier, L. Salmon, G. Molnár, A. Bousseksou, *J. Mater. Chem. C* **2017**, *5*, 4419–4425; l) V. Shalabaeva, M. Mikolasek, M. D. Manrique-Juarez, A.-C. Bas, S. Rat, L. Salmon, W. Nicolazzi, G. Molnár, A. Bousseksou, *J. Phys. Chem. C* **2017**, *121*, 25617–25621; m) K. S. Kumar, M. Studniarek, B. Heinrich, J. Arabski, G. Schmerber, M. Bowen, S. Boukari, E. Beaurepaire, J. Dreiser, M. Ruben, *Adv. Mater.* **2018**, *30*, 170516–170517; n) M. Atzori, L. Poggini, L. Squillantini, B. Cortigiani, M. Gonidec, P. Bencock, R. Sessoli, M. Mannini, *J. Mater. Chem. C* **2018**, *6*, 8885–8889; o) S. Rohlf, M. Gruber, B. M. Flöser, J. Grunwald, S. Jarausch, F. Diekmann, M. Kallane, T. Jasper-Toennies, A. Buchholz, W. Plass, R. Berndt, F. Tuczek, K. Rossnagel, *J. Phys. Chem. Lett.* **2018**, *9*, 1491–1496; p) K. Bairagi, A. Bellec, C. Fourmental, O. Iasco, J. Lagoute, C. Chacon, Y. Girard, S. Rousset, F. Choueikani, E. Otero, P. Ohresser, P. Sainctavit, M.-L. Boillot, T. Mallah, V. Repain, *J. Phys. Chem. C* **2018**, *122*, 727–731; q) L. Kipgen, M. Bernien, S. Ossinger, F. Nickel, A. J. Britton, L. M. Arruda, H. Naggert, C. Luo, C. Lotze, H. Ryll, F. Radu, E. Schierle, E. Weschke, F. Tuczek, W. Kuch, *Nat. Commun.* **2018**, *9*, 2984.
[24] a) J. A. Greer, *J. Phys. D* **2014**, *47*, 34005; b) S. Majumdar, K. Grochowska, M. Sawczak, G. Śliwiński, H. Huhtinen, J. Dahl, M. Tuominen, P. Laukkanen, H. S. Majumdar, *ACS Appl. Mater. Interfaces* **2015**, *7*, 22228; c) K. Grochowska, S. Majumdar, P. Laukkanen, H. S. Majumdar, M. Sawczak, G. Śliwiński, *Proc. SPIE 9447, 18th International School on Quantum Electronics: Laser Physics Applications* **2015**, 94470F.
[25] a) A. Piqué, *Appl. Phys. A* **2011**, *105*, 517–528; b) N. Majewska, M. Gazda, R. Jendrzejewski, S. Majumdar, M. Sawczak, G. Śliwiński, *Proc. SPIE 10453*, Third International Conference on Applications of Optics and Photonics, **2017**, 104532H.
[26] A. D. Stiff-Roberts, W. Ge, *Appl. Phys. Rev.* **2017**, *4*, 41303.
[27] a) S. Bonhommeau, G. Molnar, A. Galet, A. Zwick, J. A. Real, J. J. McGarvey, A. Bousseksou, *Angew. Chem. Int. Ed.* **2005**, *44*, 4069–4073; *Angew. Chem.* **2005**, *117*, 4137; b) T. Park, R. M. van der Veen, *Struct. Dyn.* **2017**, *4*, 044028; c) S. Cobo, D. Ostrovskii, S. Bonhommeau, L. Vendier, G. Molnár, L. Salmon, K. Tanaka, A. Bousseksou, *J. Am. Chem. Soc.* **2008**, *130*, 9019–9024.
[28] a) M. Ohba, K. Yoneda, G. Agustí, M. C. Muñoz, A. B. Gaspar, J. A. Real, M. Yamasaki, H. Ando, Y. Nakao, S. Sakaki, S. Kitagawa, *Angew. Chem. Int. Ed.* **2009**, *48*, 4767–4771; *Angew. Chem.* **2009**, *121*, 4861; b) Z. Arcís-Castillo, F. J. Muñoz-Lara, M. C. Muñoz, D. Aravena, A. B. Gaspar, J. F. Sánchez-Royo, E. Ruiz, M. Ohba, R. Matsuda, S. Kitagawa, J. A. Real, *Inorg. Chem.* **2013**, *52*, 12777–12783; c) C. H. Pham, J. Cirera, F. Paesani, *J. Am. Chem. Soc.* **2016**, *138*, 6123–6126; d) C. H. Pham, F. Paesani, *J. Phys. Chem. Lett.* **2016**, *7*, 4022–4026; e) C. H. Pham, F. Paesani, *Inorg. Chem.* **2018**, *57*, 9839–9843.
[29] a) I. Boldog, A. B. Gaspar, V. Martínez, P. Pardo-Ibañez, V. Ksenofontov, A. Bhattacharjee, P. Gütlich, J. A. Real, *Angew. Chem. Int. Ed.* **2008**, *47*, 6433–6437; *Angew. Chem.* **2008**, *120*, 6533; b) A. Mishima, T. Koshiyama, J. A. Real, M. Ohba, *J. Mater. Chem. C* **2017**, *5*, 3706–3713; c) Z.-H. Li, Y. X. Wang, W.-K. Han, W. Zhu, T. Li, Z. Li, X. Ren, Z.-G. Gu, *New J. Chem.* **2017**, *41*, 10062–10068.
[30] a) C. Bartual-Murgui, L. Salmon, A. Akou, C. Thibault, G. Molnár, T. Mahfoud, Z. Sekkat, J. A. Real, A. Bousseksou, *New J. Chem.* **2011**, *35*, 2089–2094; b) G. Molnar, S. Cobo, J. A. Real, F. Carcenac, E. Daran, C. Vieu, A. Bousseksou, *Adv. Mater.* **2007**, *19*, 2163–2167.
[31] S. Majumdar, G. Sliwinski, Y. Garcia, *In Hybrid Organic-Inorganic Interfaces: Towards Advanced Functional Materials* (Eds.: M. H. Delville, A. Taubert), **2018**, chapter 7, p. 301. vol. 2, Wiley VCH Book.

[32] K. F. Domke, D. Zhang, B. Pettinger, *J. Phys. Chem. C* **2007**, *111*, 8611–8616.
[33] G. Molnár, V. Niel, A. B. Gaspar, J. A. Real, A. Zwick, A. Bousseksou, J. J. McGarvey, *J. Phys. Chem. B* **2002**, *106*, 9701–9707.
[34] C. Bartual-Murgui, A. Cerf, C. Thibault, C. Vieu, L. Salmon, G. Molnár, A. Bousseksou, *Microelectron. Eng.* **2013**, *111*, 365–368.
[35] V. Rubio-Giménez, C. Bartual-Murgui, M. Galbiati, A. Núñez-López, J. Castells-Gil, B. Quinard, P. Seneor, E. Otero, P. Ohresser, A. Cantarero, E. Coronado, J. A. Real, R. Mattana, S. Tatay, C. Martí-Gastaldo, *Chem. Sci.* **2019**, *10*, 4038–4047.
[36] Y. Garcia, J. Moscovici, A. Michalowicz, V. Ksenofontov, G. Levchenko, G. Bravic, D. Chasseau, P. Gütlich, *Chem. Eur. J.* **2002**, *8*, 4992–5000.
[37] J. Jung, G. Schmitt, L. Wiehl, A. Hauser, K. Knorr, H. Spiering, P. Gütlich, *Z. Phys. B* **1996**, *100*, 523.
[38] T. Delgado, C. Enachescu, A. Tissot, L. Guénée, A. Hauser, C. Besnard, *Phys. Chem. Chem. Phys.* **2018**, *20*, 12493.
[39] O. Reyes-Martinez, E. Torres-García, G. Rodríguez-Gattorno, E. Reguera, *Materials* **2013**, *6*, 1452–1466.
[40] R. Tanasa, C. Enachescu, J. Laisney, D. Morineau, A. Stancu, M.-L. Boillot, *J. Phys. Chem. C* **2019**, *123*, 10120–10129.

Received: February 28, 2019